High accuracy experimental determination of copper and zinc mass attenuation coefficients in the 100 eV to 30 keV photon energy range

Yves Ménesguen, M Gerlach, B Pollakowski, R. Unterumsberger, M. Haschke, B. Beckhoff, Marie-Christine Lépy

High accuracy experimental determination of copper and zinc mass attenuation coefficients in the 100 eV to 30 keV photon energy range

Y. Ménesguen[1], M. Gerlach[2,*], B. Pollakowski[2], R. Unterumsberger[2], M. Haschke[3], B. Beckhoff[2], M.-C. Lép

[1]CEA, LIST, Laboratoire National Henri Becquerel (LNE-LNHB), 91191 Gif-sur-Yvette cedex, France

[2]Physikalisch-Technische Bundesanstalt, Abbestr. 2-12, 10587 Berlin, Germany

[3]Bruker Nano GmbH, Am Studio 2D, 12489 Berlin, Germany

[1]

Abstract

The knowledge of atomic fundamental parameters such as mass attenuation coefficients with low uncertainties, is of decisive importance in elemental quantification using X-ray fluorescence analysis techniques. Several databases are accessible and frequently used within a large community of users. These compilations are most often in good agreement for photon energies in the hard X-ray ranges. However, they significantly differ for low photon energies and around the absorption edges of any element. In a joint cooperation of the metrology institutes of France and Germany, mass attenuation coefficients of copper and zinc were determined experimentally in the photon energy range from 100 eV to 30 keV by independent approaches using monochromatized synchrotron radiation at SOLEIL (France) and BESSY II (Germany), respectively. The application of high-accuracy experimental techniques resulted in mass attenuation coefficient datasets determined with low uncertainties that are directly compared to existing databases. The novel datasets are expected to enhance the reliability of mass attenuation coefficients.

1 Introduction

Reliable knowledge of atomic properties is of high relevance in many X-ray analytical techniques. When aiming at the quantitative analysis of the elemental composition in a complex specimen, the attenuation of the emitted fluorescence lines by the main matrix elements of the sample needs to be taken into account. Several databases are accessible and frequently used within a large community of users [1, 2, 3, 4]. These compilations are based on theoretical approaches including selected experimental data and are, in general, in good agreement for photon energies in the hard X-ray range, typically above 20 keV. However, they significantly differ at low photon energies and around the absorption edges of most elements. In the frame of the European Metrology Research Programme (EMRP) project "Thin Films" (IND07), the Laboratoire National Henri Becquerel (LNHB), French national metrology laboratory for ionizing radiations and the Physikalisch-Technische Bundesanstalt (PTB), Germany's metrology institute, are jointly developing dedicated X-ray spectrometry techniques with the aim to substantially improve the reliability of selected atomic parameters and their relative uncertainties. Previous works on Cu and Zn [5, 6, 7] determined the mass attenuation coefficients and associated imaginary part of atomic form factors but focussed only on a restricted hard X-ray energy range. In this work the mass attenuation coefficients of Cu and Zn were experimentally determined in the photon energy range from 100 eV to 30 keV using monochromatized synchrotron radiation with traceable uncertainties.

[1]* current affiliation: Helmholtz-Zentrum Berlin für Materialen une Energie, Albert-einstein-Str. 15, 12489 Berlin, Germany

2 Determination of mass attenuation coefficients

The mass attenuation coefficient is the macroscopic parameter standing for the interaction probability of an X-ray photon beam in matter. It depends on the material and the photon energy and is influenced by both photo-absorption and scattering effects. The overall attenuation of a parallel and monochromatic photon beam at normal incidence in target follows the Beer-Lambert law:

$$I = I_0 \times \exp\left(-{}^{\mu}/_{\rho}\left(E\right).\rho.x\right) \tag{1}$$

where I and I_0 are the transmitted and incident photon intensities respectively, ρ (in g·cm^{-3}) and x (in cm) are respectively the target density and thickness, ${}^{\mu}/_{\rho}\left(E\right)$ is the energy-dependent mass attenuation coefficient in cm^2·g^{-1}. A convenient way to determine the mass attenuation coefficients, ${}^{\mu}/_{\rho}$, is in transmission mode, using a monochromatic photon beam of low divergence that can be produced by a synchrotron light source with dedicated optics. The basic method is to measure the photon flux (I_0) in front of the sample and just behind it (I) thus :

$${}^{\mu}/_{\rho}\left(E\right) = -\frac{1}{\rho.x} \times \ln\left(\frac{I}{I_0}\right) \tag{2}$$

Consequently, the final uncertainty budget is linked to the target characteristics and the photon flux intensities. A study of the uncertainty budget associated with the counting statistics led Nordfors [8] to establish a criterion to minimize the statistical uncertainty. Best results are obtained for samples with a thickness which satisfies: $2 \leq \ln\left(I_0/I\right) \leq 4$. To achieve absorption of X-rays for such measurement, sample thicknesses have to be in the order of magnitude of some micrometres and sometimes less than a micrometre in case of soft X-rays.

2.1 Methodology at LNHB

The experimental determination of mass attenuation coefficients is carried out in two steps.

2.1.1 Characterization of the samples

As a first step, accurate values of the sample characteristics are determined. The metal foil targets are supplied by Goodfellow corporation [9] and are selected with a purity better than 99.9 %. Measuring absolute mass attenuation coefficients requires the knowledge of the number of atoms interacting with the photon beam. To derive absolute values for the mass attenuation coefficients from equation 2, density and thickness must be known with the best possible uncertainty budget. It appeared to be difficult to measure a thickness in the range of micrometres or less with accurate techniques independent from X-ray transmission measurements which rely on mass attenuation coefficients. The sample preparation technique could also add an important bias on the density value from bulk: laminated foils or deposited materials with any technique could end up with several percents deviation from tabulated bulk density. Equation 2 can be re-written in:

$${}^{\mu}/_{\rho} = -\frac{1}{\rho.x} \times \ln\left(\frac{I}{I_0}\right) = -\frac{A}{M} \times \ln\left(\frac{I}{I_0}\right) = -\frac{A}{M} \times \ln\left(T\right) \tag{3}$$

where M is the mass of the sample in g, A its area in cm^2 and T the transmittance. Measuring the mass and area of the samples has the advantage to be more accurate and independent from X-ray analysis techniques. The remaining sources of inaccuracies are the roughness and thickness homogeneity of the samples that have to be evaluated. The mass is weighed with a calibrated microbalance used in a room of which ambient air hygrometry, temperature and pressure are controlled, giving an absolute uncertainty of 9 µg at best. The area is measured with a vision machine consisting of a microscope with two calibrated stages and a picture analyser. It allows several magnifications in order to provide an adequate enlargement necessary to follow with accuracy a complicated shape, reducing the associated relative uncertainty below 0.1 %.

Copper samples characteristics Three samples of different thicknesses were chosen (Tab. 1) in order to have a measurable transmitted flux and fulfilll the Nordfors criterion in the energy range from 3.5 keV up to 30 keV.

N°	nominal thickness / µm	mass / mg	area / mm^2	purity (mass fraction) / %
1	3.8	2.996(10)	86.84(5)	99.97
2	5	12.686(10)	255.99(7)	99.97
3	20	42.194(10)	253.33(7)	99.99

Table 1: Characteristics of copper samples used at LNHB

Mass per unit area of the whole sample is an average and one should check if the spot used in the transmittance measurement procedure is representative of the sample. A mapping was done with a 2D micro-XRF machine (BRUKER M4 Tornado). The X-ray tube was set at 50 kV with an emitting current of 200 µA. The step size between each pixel is 150 µm. A spectrum was recorded at each step and the Cu K_α (summed from 7.91 keV to 8.16 keV) line intensity was derived. The results are presented on figure 1 in false colors. The small inhomogeneities revealed by this technique may be due to the rolling during the manufacturing process of the films. The blue square represents the spot used in transmittance measurements. The average intensity of the square used for the transmittance measurements was compared to the average intensity of the total sample and small relative differences of 0.5 % and 0.2 % were found respectively for the 5-µm and 20-µm thick samples.

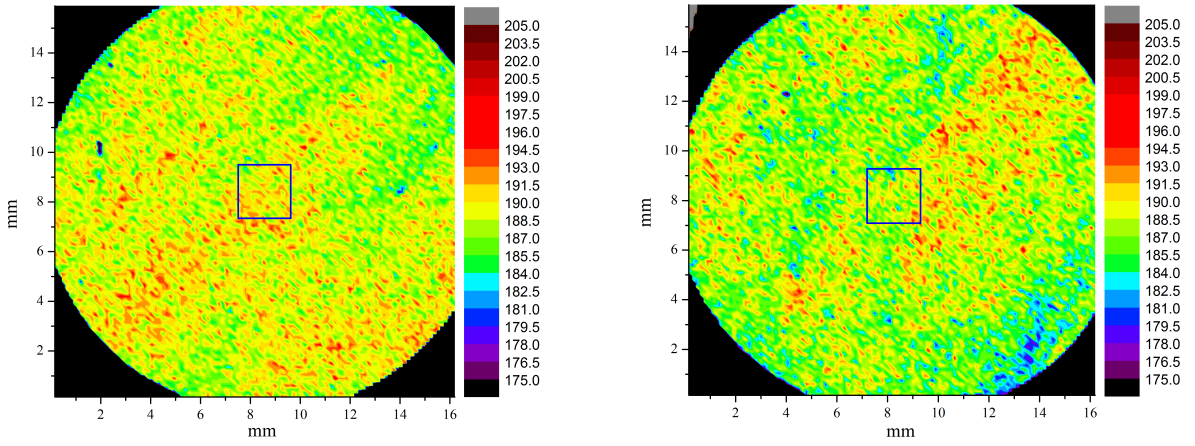

Figure 1: Left: Homogeneity of the 5 µm-thick Cu sample. Right: Homogeneity of the 20 µm-thick Cu sample. The color code corresponds to the linear scale of the Cu-K fluorescence radiation intensity recorded. The blue square shows the spot used in the transmittance measurements procedure

Zinc samples Two samples of different thicknesses were chosen (Tab. 2) in order to have a measurable transmitted flux in the energy range from 3.5 keV up to 30 keV.

N°	nominal thickness / µm	mass / mg	area / mm^2	purity (mass fraction) / %
1	10	11.134(10)	156.37(7)	99.9
2	20	20.828(10)	156.43(7)	99.9

Table 2: Characteristics of zinc samples used at LNHB

The sample surface mapping was done for these two Zn samples. The step size between each pixel is 100 µm. A spectrum was recorded at each step and the Mo K_α (summed from 17.28 keV to 17.58 keV) line intensity produced by the sample holder and transmitted by the sample were derived. The results are presented on figure 2 in false

colors, where the blue square represents the spot used in transmittance measurements. The average intensity of this spot was compared to the average intensity of the total sample and relative differences of 0.2 % and 0.1 % were found for the 10-µm and 20-µm thick samples, respectively.

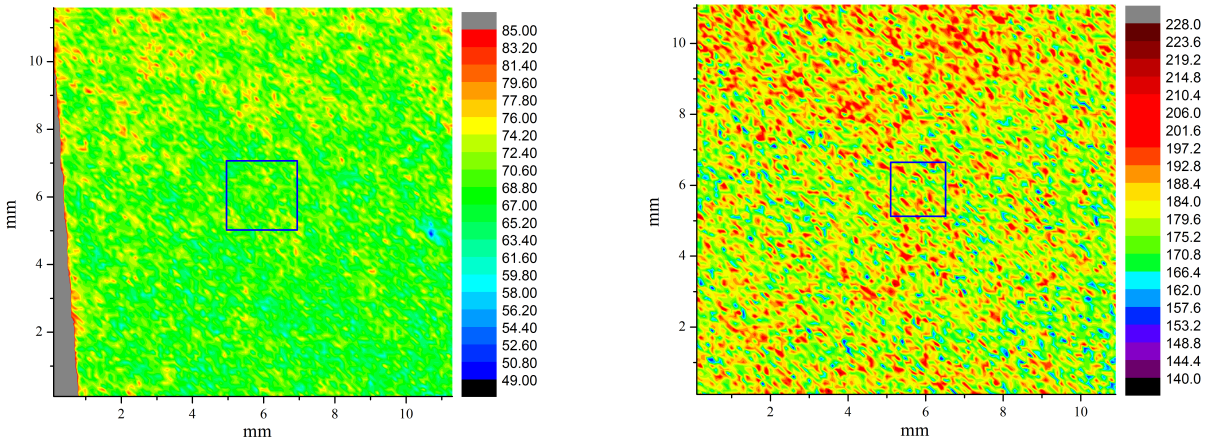

Figure 2: Left: Homogeneity of the 10 µm-thick Zn sample. Right: Homogeneity of the 20 µm-thick Zn sample. The color code corresponds to the linear scale of the Zn-K fluorescence radiation intensity recorded. The blue square shows the spot used in the transmittance measurements procedure

2.1.2 Transmittance measurements

The second step is the X-ray transmission measurement, using the procedures described in detail in [10]. Experiments were performed at the Metrology beamline at SOLEIL synchrotron, France (proposal number 20121288) on the hard X-rays branch. For a reliable measurement, i.e. with an uncertainty budget as low as possible, one has to know I and I_0 with high accuracy. Different parameters must then be checked to ensure measurement with low uncertainties, such as the beam quality (stability, monochromaticity and stray light) ensured by the Si(111) double crystal monochromator.

Flux stability The relative fluctuation of the flux intensity is better than 0.4 % due to the synchrotron top-up mode (Fig. 3 left). As the attenuation measurements are done by measuring the transmitted flux I and the incoming flux I_0 sequentially, an interval of about 60 s is necessary to remove the sample from the beam. The worst case appears when a new injection of electrons in the storage ring happens between the two necessary measurements thus giving the maximum deviation in the flux intensity measurement.

Monochromaticity The Bragg angle of the monochromator device is equipped with a rotary position encoder that needs a calibration reference. An accurate calibration of the energy axis of the monochromator is obtained by using several metal foils as transmission targets and energy scanning around their absorption edge energies. The first derivative of these transmission measurements is used to derive the accurate transition energy, then the Bragg formula gives the corresponding angle. The correct absolute angle is found using the absorption edge energies provided by the table from Deslattes et al. [11], also derived from the Bragg formula. The comparisons between the absolute angles gives an offset that is provided to the monochromator device. The residual difference between the angular position given by the encoder and the values derived from the tabulated absorption edges is presented on Fig. 3 right and is kept below 0.04 %.

Higher harmonics and continuous stray light contributions Photons that are not at the target photon energy originate either from higher order harmonics that are reflected as well by the double crystal monochromator following the Bragg law, starting with third harmonics for Si(111) or from parasitic reflections of the incident bending

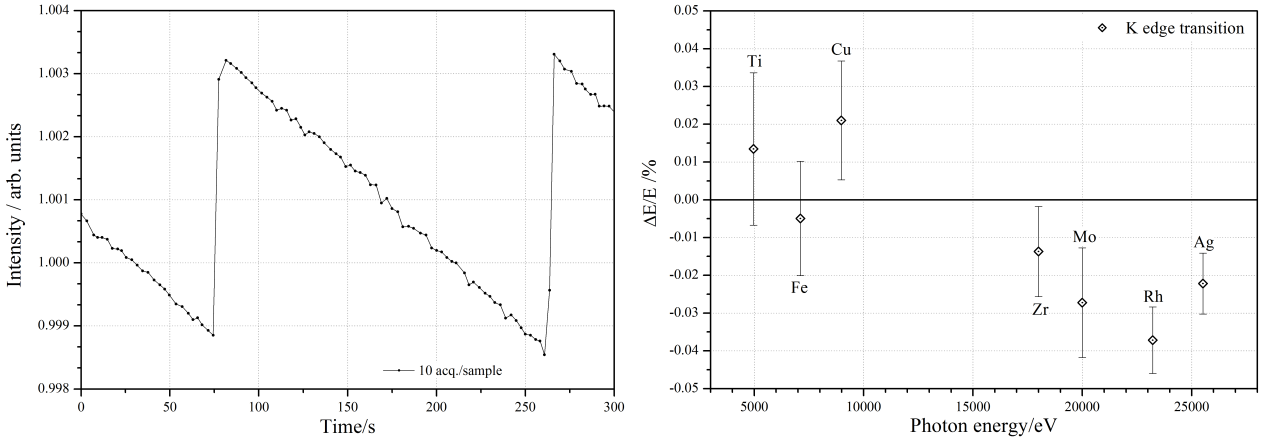

Figure 3: Left: Flux fluctuations at 9 keV. Right: Percentage difference between calibrated energies and absorption edge energies from the Deslattes table.

magnet radiation or white beam which are called stray light contributions. The contributions of the harmonics are significant below 7 keV as shown by the experimental points in table 3. These values are compared to a theoretical approach using the XRVision 2.0 software, using the synchrotron radiation characteristics, beamline geometry and optics characteristics. In these cases, a small detuning of the second monochromator crystal is necessary for energies below 7 keV to avoid higher-order harmonics [12] and the total contribution of higher-order harmonics is reduced to 0.1 %.

photon energy (eV)	% 1^{st} harmonics (exp.)	% 1^{st} harmonics (theory)
3000	0.941 (5)	0.942
4000	0.968 (11)	0.958
6000	0.992 (8)	0985
8000	0.997 (2)	0.992

Table 3: Contribution of first harmonics to the total number of photons with parallel crystals of the monochromator. The theoretical values are calculated with XRVision 2.0 software.

The contribution to incoming flux of stray light, i.e. unwanted reflected photons with energies covering all the white beam spectrum, is difficult to measure precisely. Diodes cannot discriminate between energies and energy-dispersive detectors (EDS) are not suitable as well: the peak/background ratio of EDS is not high enough to reach the sufficient order of magnitude between the photon counts at energy of interest and at any other energy. Nevertheless, we can use the transmittance measured for samples with different thicknesses in the same energy range to estimate the stray light contribution to the uncertainty budget. If there is no stray light contribution, the transmittance measured for a sample should be equal to the one obtained for the same thickness from the transmittance of a second sample of different thickness using the ratio of their masses per unit area.

Due to the experimental conditions, not all the photon energy range available at the beamline is relevant. The photon flux is measured by means of an X-ray photodiode. At a photon energy E, its current is determined by the product of the spectral distribution of photons due to the dipole characteristics, the beamline geometry and transmission characteristics (crystals reflectivities, filters) and the photodiode efficiency. Using the same software as previously, we calculate for the worst case (i.e. the double crystal monochromator is in perfect Bragg condition) the possible contribution of third harmonics (first dominating harmonics with a Si(111) double crystal monochromator) to the overall photodiode photocurrent in the experimental conditions with the selected samples used as filters. The results are presented on figure 4 (left). These simulation results suggest to compare the transmittance of foils at photon energies larger than the K absorption edge energy in order to isolate stray light from higher-order harmonics.

As we expect the stray light contribution to be independent from the photon energy selected (or Bragg angle), which is not the case for harmonics, the estimation of its contribution can be made in a photon energy range free of higher-order harmonics. In order to isolate the stray light contribution, we calculate from the measured transmittance of several copper foils with various thicknesses, in the same photon energy range, the transmittance that would be obtained for the thickness of another foil taken as reference. We use copper samples with nominal thicknesses of 5, 10, 20 and 50 µm (mass and area were measured as for other samples). The experiment covers the photon energy range from 13 keV up to 29 keV. The ratio R of the transmittance T obtained with sample 1 (T_1) for the thickness of sample 2 to the transmittance of sample 2 (T_2) is expressed as follows:

$$R = \frac{T_1^{\left(\frac{M_2/A_2}{M_1/A_1}\right)}}{T_2} \tag{4}$$

where M_1 and M_2 are the masses of sample 1 and 2 respectively and A_1 and A_2 their respective area. The figure 4 (right) represents the ratio R for the $^{10}/_{5}$, $^{20}/_{10}$ and $^{50}/_{20}$ comparisons. If a significant contribution of stray light was present, we would expect these ratios to be less than 1 as the thicker sample should attenuate more X-rays. The results do not show any tendency and this experimental methodology is limited here by the statistical noise. Furthermore, complementary measurements done with a spectrometer did not show any photon contribution at different energies than first and higher harmonics, which means that stray light is reduced below the limit of detection of the spectrometer, which is roughly given by its peak/background ratio capability (several10^3).

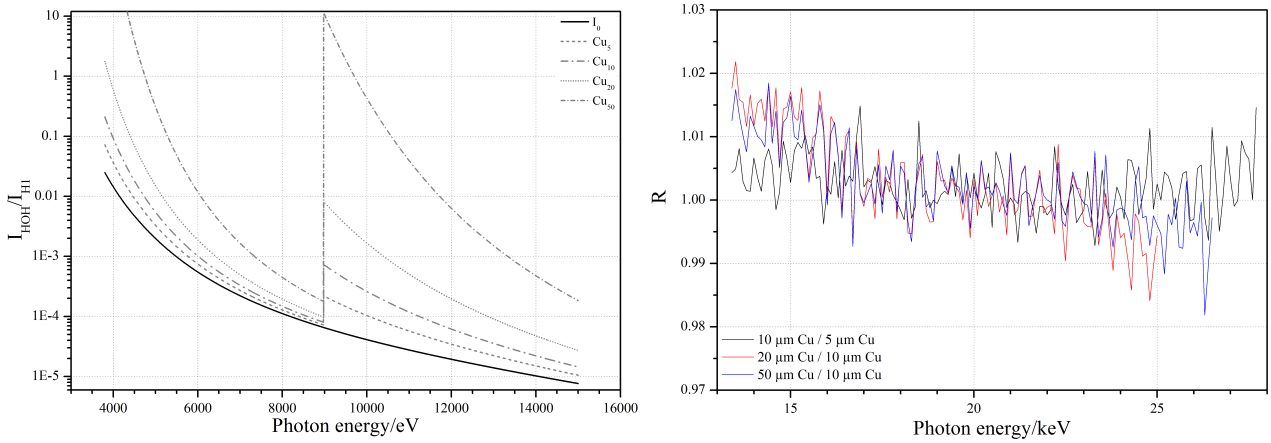

Figure 4: Left: ratio of the higher-order harmonics (HOH) to the first harmonics in terms of the diode current, theoretical approach using XRVision 2.0 software. Thick line is without any sample (I_0) and other lines are representing the cases with copper samples of various thicknesses (Cu_x). Right: ratio of transmittances between samples of different thicknesses.

Experimental procedure Once the energy calibration is achieved, long scanning sequences with a maximum 25 eV step can be done with steps of 1 eV around the K absorption edge energies of copper and zinc and 5 eV to several tens of eV above. The transmittance measurements are done using a beam collimated at 2×2 mm^2 or 3×3 mm^2 thus considering these areas representative of the thickness of the whole target. The transmitted and incident photon intensities, I and I_0 respectively are recorded by mean of an AXUV:Al photodiode, each value being an average of 10 samples from the Keithley 6517 running in amperemetre mode. An average measurement of the dark noise is substracted to each photodiode current values in order to derive an unbiased transmittance parameter in equation 3.

2.1.3 Evaluation of uncertainties

To evaluate the uncertainty of the experimental mass attenuation coefficients, equation 3 was derived according to all the influence quantities mentioned in the "Guide to the expression of uncertainty in measurement" [13]. Finally, the transmittance measurement combines the contribution from the stray light and harmonics, flux stability and photodiode intensity measurements. The relative uncertainty corresponding to the transmittance measurement is evaluated as the standard deviation from the measurements and a smoothed curve of the transmittance. The purity of the sample can be very difficult to translate into correction terms or uncertainties as a lot of different atoms can be present at very low concentrations. Moreover, the main impurity may not be the one with the most significant attenuation effect at any photon energy. So we establish an upper limit to the relative uncertainty associated with impurities. Equation 3 then transforms into:

$$(\mu/\rho)_0 = -\frac{A}{m_0} \times \left(\ln(T) + \frac{\sum_i (\mu/\rho)_i \times m_i}{A} \right) \tag{5}$$

where the subscript 0 stands for the element of interest and the traceable impurities are designated by the subscript i. We introduce the purity parameter P as the mass fraction of the element of interest as given in tables 1 and 2. This leads to $m_0 = M \times P$ and $\sum_i m_i = M \times (1-P)$. We also introduce the parameters α and β that are the greatest and the lowest ratios of the mass attenuation coefficients of an impurity to the element of interest respectively. For example, in the case of copper with a silver impurity, α can be found just below the K absorption edge energy (the mass attenuation value is low for copper and large for silver). This gives limits to the second term in equation 5:

$$\beta \times (\mu/\rho)_0 \times M \times (1-P) \quad \leqslant \quad \sum_i (\mu/\rho)_i \times m_i \quad \leqslant \quad \alpha \times (\mu/\rho)_0 \times M \times (1-P) \tag{6}$$

Finally, combining equations 5 and 6:

$$-\frac{A}{M \times (\alpha + P \times (1-\alpha))} \times \ln(T) \leqslant (\mu/\rho)_0 \leqslant -\frac{A}{M \times (\beta + P \times (1-\beta))} \times \ln(T) \tag{7}$$

The error between the measured value of the mass attenuation coefficient (μ/ρ) and the true one $(\mu/\rho)_0$ is defined as $\Delta\mu/\rho = (\mu/\rho) - (\mu/\rho)_0$, and combined with equation 7, this gives limits to the uncertainty of the mass attenuation measurement due to impurities:

$$\frac{(\beta-1) \times (1-P)}{P + \beta \times (1-P)} \leqslant \frac{\Delta\mu/\rho}{\mu/\rho} \leqslant \frac{(\alpha-1) \times (1-P)}{P + \alpha \times (1-P)} \tag{8}$$

In order to simplify the evaluation of the uncertainties associated with impurities and because it is a minor contribution, the mass attenuation coefficient can be rewritten as:

$$\mu/\rho = -\frac{A}{M} \times \ln(T) \times k_p$$

where $k_p = 1$ stands for the correction factor for impurities in the sample and has an associated relative uncertainty given by the largest value of the two terms in equation 8 (in absolute value). The associated uncertainties come from the sample characteristics and from the X-ray beam quality and are combined as follows:

$$\left(\frac{u(\mu/\rho)}{\mu/\rho} \right)^2 = \left(\frac{u(M)}{M} \right)^2 + \left(\frac{u(A)}{A} \right)^2 + \frac{\left(\frac{u(T)}{T} \right)^2}{(\ln(T))^2} + \left(\frac{u(k_P)}{k_P} \right)^2 \tag{9}$$

Among other issues, this expression means that uncertainties directly related to transmission measurements are providing the lowest uncertainties with respect to the mass attenuation coefficients and cannot be further reduced. Table 4 gives the different contributions to the overall combined uncertainty budget of the mass attenuation coefficient measurements for both copper and zinc samples. Finally, the combined uncertainty budget is most often kept below 1 % and rarely exceeds 1.2 %. Figure 5 presents the results of the combined uncertainty budget as a function of photon energies.

contribution	Cu sample 1	Cu sample 2	Cu sample 3	Zn sample 1	Zn sample 2
mass	0.33 %	0.072 %	0.023 %	0.087 %	0.047 %
area	0.053 %	0.027 %	0.026 %	0.044 %	0.044 %
sample purity	0.1 %	0.1 %	0.1 %	0.57 %	0.57 %
sample homogeneity		0.5 %	0.2 %	0.2 %	0.1 %
transmittance	0.17 %	0.26 %	0.26 %	0.29 %	0.37 %
energy calibration	< 0.04 %	< 0.04 %	< 0.04 %	< 0.04 %	< 0.04 %

Table 4: Relative standard uncertainties contributing to the total uncertainty budget at LNHB

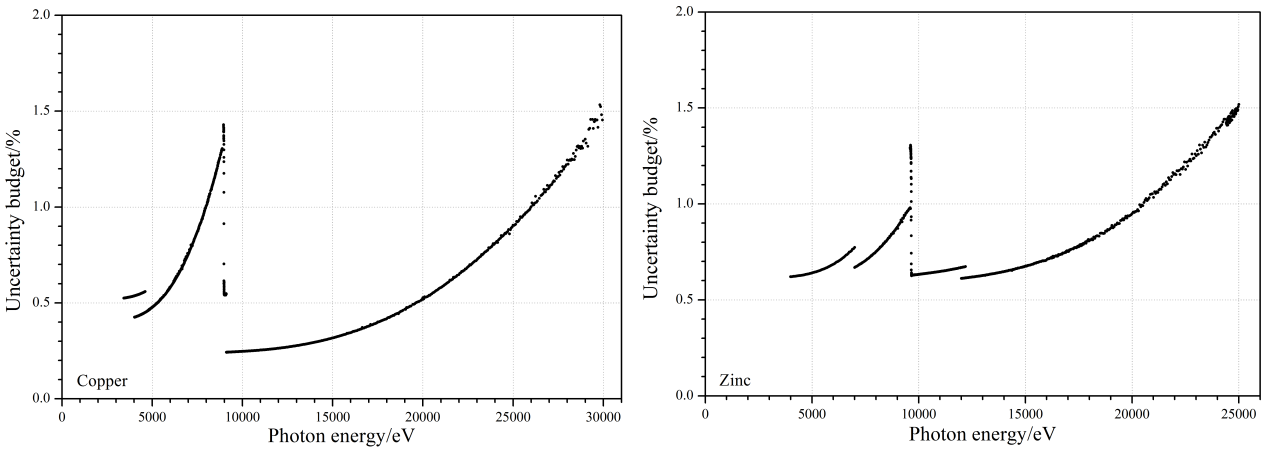

Figure 5: Uncertainty budget associated with the mass attenuation coefficients of Cu (left) and Zn (right).

2.2 Methodology at PTB

Independent transmittance measurements were carried out at the laboratory of PTB at the electron storage ring BESSY II in Berlin (Germany) to cover the low energy photon range between 100 eV and 1 keV. Monochromatized synchrotron radiation of high spectral purity was used for transmission measurements of five copper foils with nominal thicknesses of 50 nm, 500 nm, 3 µm, 10 µm and 100 µm, respectively. Measurements for photon energies between 100 eV and 1860 eV were performed at an undulator beamline, equipped with a plane grating monochromator [14] or at the SX700 bending magnet beamline [15], also equipped with a plane grating monochromator. A key advantage of the monochromator beamline for undulator radiation is the provision of radiant power that is one to three orders of magnitude higher than the one of the bending magnet monochromator beamline. In addition, a slight detuning of the undulator harmonic energy against the plane grating monochromator allows for an improved higher-order suppression capability in conjunction with the red shift of higher-order harmonics of the undulator. To further reduce higher-order contributions dedicated absorption filters are used between exit slit and image focal plane. Stray light contributions of about 0.5 % to 1 % have to be taken into account depending on the operational parameters. The uncertainty of the energy scale of the plane grating monochromators is in the 10^{-4} range. For photon energies from 1.8 keV up to 10 keV a four-crystal monochromator beamline [16] with high-order suppression capabilities in the range of 10^{-4} to 10^{-7} was used. For hard X-rays in the photon energy range above 10 keV additional measurements at a 7 T wavelength-shifter beamline (WLS) [17], which shifts the critical energy of a bending magnet from 2.5 keV to more than 13 keV, were performed using a double-crystal monochromator at the BAMline. To reduce higher order contributions an additional double-multilayer monochromator was used in series for photon energies below 20 keV. In order to reduce stray light contributions below the 1 % level several dedicated absorption filters are employed at the BAMline. At all beamlines calibrated instrumentation, such as semiconductor photodiodes, calibrated against a cryogenic radiometer as primary detector standard [18], were employed. Measurements were performed in an ultra-high vacuum chamber equipped with a 9-axis manipulator [19]

that allows for a precise alignment of the respective samples.

The transmittance was measured with a maximum step width of 25 eV. At the L-edges of Cu the resolution was reduced to 0.5 eV, and at the K-edge of Cu to 1 eV. In order to reveal absolute values for the mass attenuation cross sections, PTB employed the following procedure: very similar foils as the one used by LNHB were measured in the entire photon range of interest in the current study. Then, mass attenuation coefficients determined by LNHB were matched by PTB measurements in the hard X-ray range resulting in an estimated uncertainty contribution of 1.0 %. At the transition from the hard to the soft X-ray range at 1.8 keV an additional uncertainty contribution of about 1.0 % has to be assumed for the low energy mass attenuation cross sections at PTB. In conjunction with transmittance uncertainties of 0.5 %, higher-order contributions and stray light contributions of 1.0 %, the cross sections derived from PTB measurements are affected with combined uncertainties of 1.5 % in the hard and 1.8 % in the soft X-ray ranges, respectively.

3 Experimental results and discussion

3.1 Absolute mass attenuation coefficients of Copper and Zinc

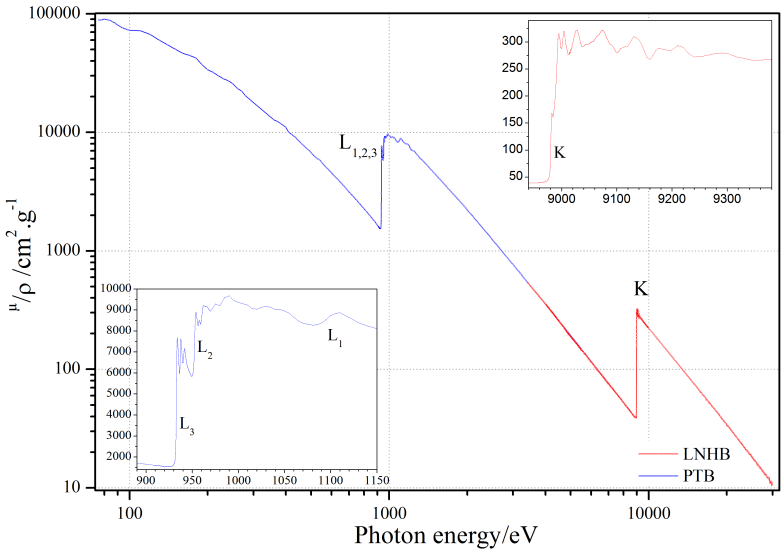

Figure 6: Mass attenuation coefficients of Cu with a resolution of 25 eV, 1 eV around the K absorption edge energy and 0.5 eV around the L-edges.

The measurements carried out by LNHB and PTB resulted in a set of transmission data for copper and zinc from which the energy dependent mass attenuation coefficients were calculated. In the case of copper, the photon energy range starts from 100 eV and goes up to 30 keV (Fig. 6), covering both K- and L- absorption edges (Insets in Fig. 6 present a closer view around the absorption edges). In the case of zinc, the measurements cover a photon energy range from 440 eV to 25 keV (Fig. 7 with a closer view around the absorption energies).

A comparison of the experimental values obtained independantly from both institutes is of high interest as it gives an other point of view about the estimated uncertainties associated with instrumental and experimental contributions quoted. Because, both institutes did not measure the mass attenuation coefficients at the exact same photon energies, we interpolated the most comprehensive set of data to the energy points of the second set in order to add a minimum bias from the interpolation method. We then derive a standard deviation by range of 2 keV below the K- absorption edge of both elements. In the case of copper, the standard deviation is 0.8 %, 0.9 % and 0.9 % between 3.4 keV and 5 keV, 5 keV and 7 keV and 7 keV and the K absorption edge energy respectively. In the case of zinc, the standard deviation is 0.4 %, 0.9 % and 1.6 % between 4 keV and 6 keV, 6 keV and 8 keV and 8

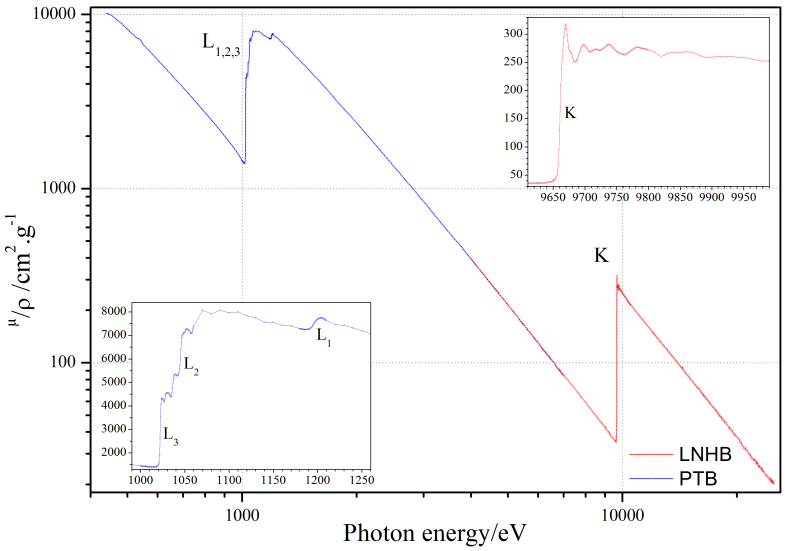

Figure 7: Mass attenuation coefficients of Zn with a resolution of 25 eV down to 1 eV around the K absorption edge energy and 0.5 eV around the L-edge.

keV and the K absorption edge energy respectively. These values are all well in line with the quoted uncertainties provided by both institutes.

3.2 X absorption fine structures (XAFS) simulations

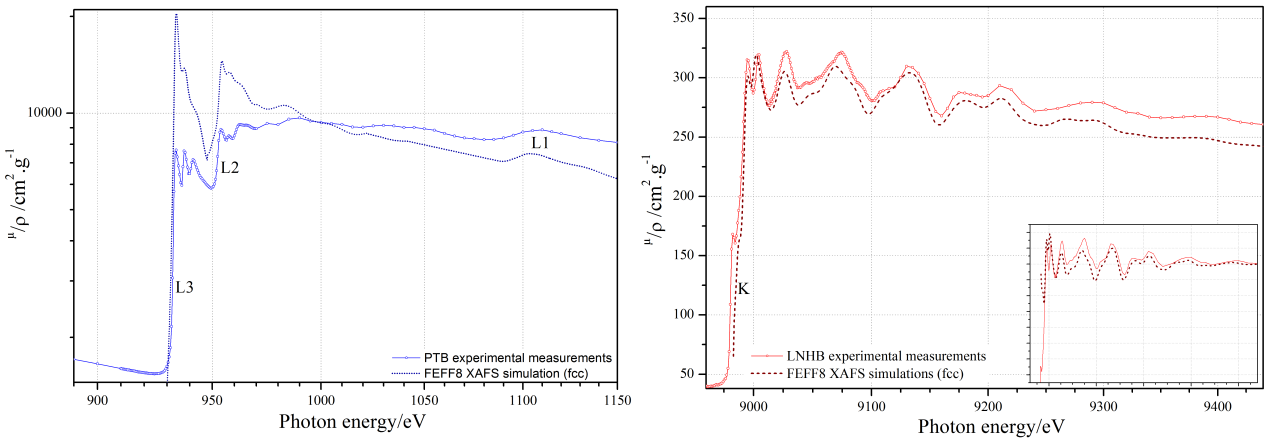

Figure 8: Left: Mass attenuation coefficients of Cu around the L-absorption edge. Right: XANES and EXAFS above the K-absorption edge

When performing transmittance measurements over a very broad spectral range, it would be most appropriate to have very similar foils regarding crystallinity and chemical species. The impact of crystallinity on the run of the curves is mainly observable in the vicinity of the X-ray absorption edges by slight deviations. When different crystallinity may occur for foils of different thicknesses, e.g. due to their production process, theoretical calculations may help to identify coordination or speciation states, thus allowing for attributing specific edge regions to probable coordination states. Ab-initio calculations for the near-edge regions of the Cu L and K edges have been performed

with FEFF8.4 [20] assuming metallic cooper in cubic phase. Figure 8 presents the calculated data together with the experimental ones. The inset graph presents the same values with the same photon energy scale thus removing the constant offset in order to compare only the fine structures. Comparing both experimental and theoretical data, the runs of the curve for Cu K edge are in good agreement which validates the assumed crystalline phase. But for the Cu L edges the agreement is rather poor. This can be explained because, the measurements in the soft x-ray range demand very thin foils for transmission measurements. Unfortunately, such thin foils are neither commercially available nor easily producible and manageable. Here, the analyzed Cu foil is too thick for this purpose and the resulting experimental data are partially dominated by self-attenuation effects [21]. Moreover, ab-initio calculation with FEFF8.4 are very challenging for Cu L edges.

In the case of Zn, once again, ab-initio calculations of XAFS performed with FEFF8.4 [20] above all edges of metallic zinc in hexagonal close-packed phase is presented together with the experimental data. If the amplitude of the oscillations are in good agreement above the K-edge, they are a bit discrepant above L_3 and L_2 edges, nevertheless the shapes of the oscillations are in good concordance

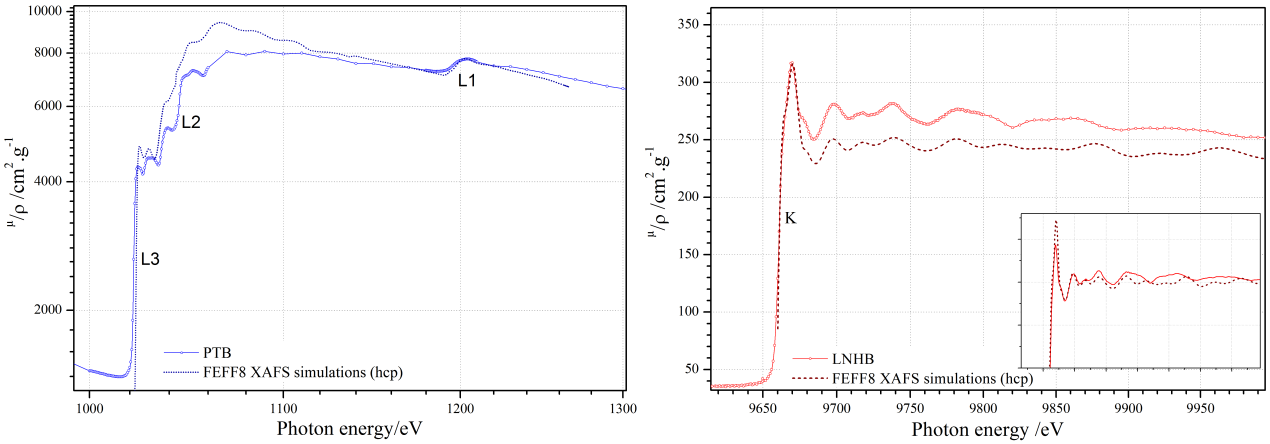

Figure 9: Left: Mass attenuation coefficients of Zn around the L-absorption edge. Right: XANES and EXAFS above the K-absorption edge

4 Comparisons with published values and databases

The results of the current work are compared to theoretical or experimental values compiled in other published databases such as [1, 2, 3, 4, 22] as well as the most recent experimental works [5, 6, 7]. The differences between the new measurements and other tabulated values are presented in figures 10 and 11. These graphs plots the relative deviation as follows:

$$\frac{\Delta\mu}{\mu} = \frac{\mu_{EXP} - \mu_{DB}}{\mu_{DB}} \times 100 \tag{10}$$

where μ_{EXP} stands for our experimental mass attenuation coefficients measurements and μ_{DB} stands for values from a published database. It shows a clear tendency above the K-absorption edge where the experimental values are larger by up to 5 %, thus showing considerably larger deviations than one may expect from the uncertainties of the current work and some of those stated in the respective works of other authors. More unexpected is the difference of a few percents between the experimentally determined values and those of existing databases in the 2 keV to 5 keV photon energy range for copper. Our experimental works are however in good agreement with many of the works of other authors and extend the spectral range to soft x-rays as compared to some of these works. In the case of zinc, it shows a clear tendency above the K-absorption edge where our experimental values are larger by up to 10 %. A small difference of about 2 % is also noticable in the 3 keV to 9 keV photon energy range. The larger differences have to be stated around and below the L-edges.

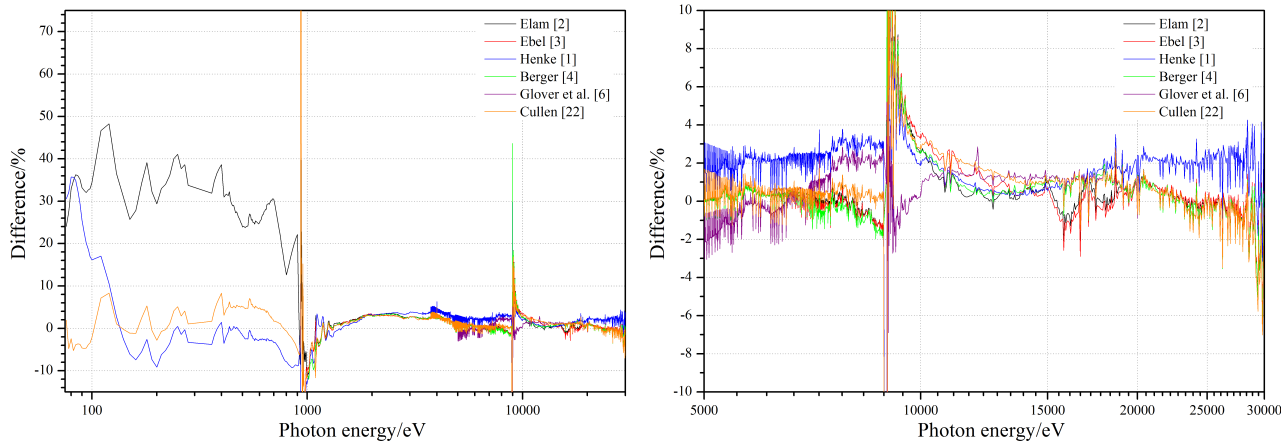

Figure 10: Comparison between compiled values of mass attenuation coefficients of Cu from PTB and CEA/LNHB and published data bases.

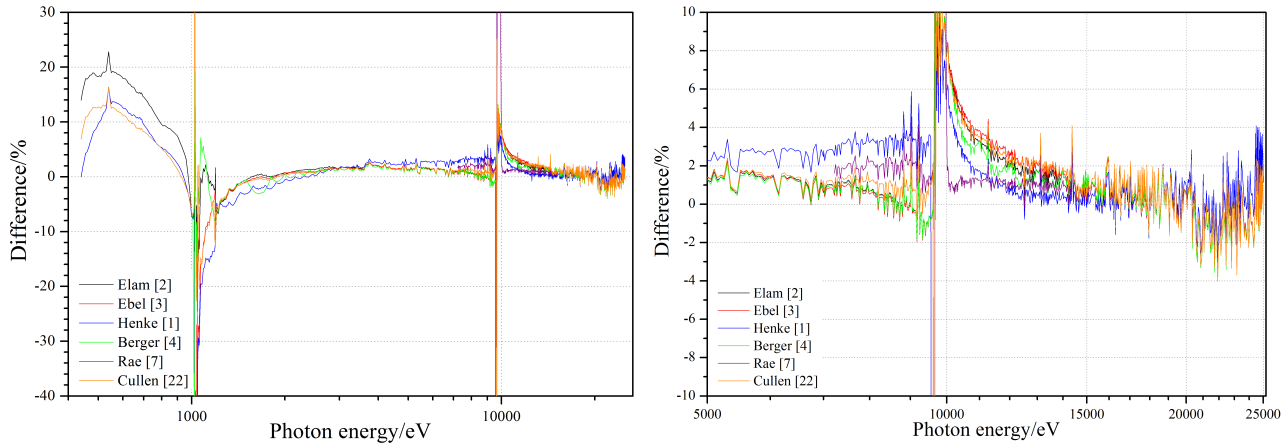

Figure 11: Comparison between compiled values of mass attenuation coefficients of Zn from PTB and CEA/LNHB and published data bases.

5 Conclusion

Two full sets of atomic fundamental parameters, that are the mass attenuation coefficient of Cu and Zn in the photon energy range from 100 eV to 30 keV, have been determined by LNHB and PTB from independent experiments partially in the same spectral range, in order to take care of any systematic and statistical errors. The respective results were directly compared and a good agreement with respect to the uncertainties was found within the whole photon energy ranges of interest, here. Deviations from tabulated values above the K-edge of Cu and Zn were found to be up to 10 % and are even larger in the low photon energy range. Comparison with accessible data bases such as that published by Berger [4], Henke [1], Cullen [22], Elam [2] or Ebel [3] indicates a potentially relevant improvement of accuracy, especially around the K- and L-absorption edges. At very low photon energies, the uncertainties slightly increase. For very thin foils undesired surface contamination or oxide cap layers are to be included in the evaluation of transmittance measurements. The improved reliablity of the uncertainty budget of the results achieved in the present work can be expected to substantially support validation procedures as well as several modern application fields to which quantitative X-ray fluorescence analysis can contribute.

Acknowledgements

The authors are grateful to the European Metrology Research Program (EMRP) within the project IND07 Thin Films. "The EMRP is jointly funded by the EMRP participating countries within EURAMET and the European Union". LNHB authors are grateful to Pascal Mercere and Paulo Da Silva for assistance on the metrology beamline and to the SOLEIL staff for smoothly running the facility. PTB authors gratefully acknowledge the support of Christian Laubis and Christian Stadelhoff for the experiments at SX700 beamline as well as the support by Jan Weser and Cornelia Streeck regarding the experiments at the FCM beamline and the BAMline.

References

[1] B. L. Henke, E. M. Gullikson, and J. C. Davis, "X-ray interactions: photoabsorption, scattering, transmission, and reflection at E = 50-30000 eV, Z = 1-92," *Atomic Data and Nuclear Data Tables*, vol. 54, no. 2, pp. 181–342, 1993.

[2] W. T. Elam, B. D. Ravel, and J. R. Sieber, "A new atomic database for X-ray spectroscopic calculations," *Radiation Physics and Chemistry*, vol. 63, pp. 121–128, 2002.

[3] H. Ebel, R. Svagera, M. F. Ebel, A. Shaltout, and J. H. Hubbell, "Numerical description of photoelectric absorption coefficients for fundamental parameters programs," *X-Ray Spectrometry*, vol. 32, no. 6, pp. 442–451, 2003.

[4] M. J. Berger, J. H. Hubbell, S. M. Seltzer, J. Chang, J. S. Coursey, R. Sukumar, and D. S. Zucker, *XCOM: Photon Cross Section Database (version 3.1)*, National Institute of Standards and Technology Std., 2010, consultation date: 2015. [Online]. Available: http://physics.nist.gov/xcom

[5] C. T. Chantler, C. Q. Tran, D. Paterson, D. Cookson, and Z. Barnea, "X-ray extended-range technique for precision measurement of the x-ray mass attenuation coefficient and im(f) for coper using synchrotron radiation," *Physics Letters A*, vol. 286, pp. 338–346, 2001.

[6] J. L. Glover, C. T. Chantler, Z. Barnea, N. A. Rae, C. Q. Tran, D. C. Creagh, D. Paterson, and B. B. Dhal, "Measurement of the x-ray mass-attenuation coefficient and imaginary component of the form factor of copper," *Physical Review A*, vol. 78, p. 052902, 2008.

[7] N. A. Rae, C. T. Chantler, Z. Barnea, de Jonge M. D., C. Q. Tran, and J. R. Hester, "X-ray mass attenuation coefficients and imaginary components of the atomic form factor of zinc over the energy range of 7.2-15.2 keV," *Physical Review A*, vol. 81, pp. 1–10, 2010.

[8] B. Nordfors, "The statistical errors in X-ray absorption measurements," *Arkiv Fysik*, vol. 18, pp. 37–47, 1960.

[9] Goodfellow Cambridge Limited (GB). Consultation date: 2015. [Online]. Available: http://www.goodfellow.com/home.aspx

[10] Y. Ménesguen and M.-C. Lépy, "Mass attenuation coefficients in the range $3.8 \leq E \leq 11$ kev, K fluorescence yield and K_β/K_α relative X-ray emission rate for Ti, V, Fe, Co, Ni, Cu, and Zn measured with a tunable monochromatic X-ray source," *Nuclear Instruments & Methods In Physics Research B*, vol. 268, no. 16, pp. 2477–2486, 2010.

[11] R. D. Deslattes, E. G. Kessler, P. Indelicato, L. de Billy, E. Lindroth, and J. Anton, "X-ray transition energies: new approach to a comprehensive evaluation," *Reviews of Modern Physics*, vol. 75, no. 1, pp. 35–99, 2003.

[12] Y. Ménesguen and M.-C. Lépy, "Characterization of the Metrology beamline at the SOLEIL synchrotron and application to the determination of mass attenuation coefficients of Ag and Sn in the range $3.5 < E < 28$ keV," *X-Ray Spectrometry*, vol. 40, no. 6, pp. 411–416, 2011.

[13] JCGM, *Evaluation of measurement data - Guide to the expression of uncertainty in measurement.* BIPM, 2008, consultation date: 2015. [Online]. Available: http://www.bipm.org/fr/publications/guides/gum.html

[14] F. Senf, U. Flechsig, F. Eggenstein, W. Gudat, R. Klein, H. Rabus, and G. Ulm, *Jounal of Synchrotron Radiation*, vol. 5, p. 780, 1998.

[15] F. Scholze, B. Beckhoff, G. Brandt, F. Fliegauf, A. Gottwald, R. Klein, B. Meyer, D. Rost, U. Schwarz, R. Thornagel, J. Tümmler, K. Vogel, J. Weser, and Ulm, "High-accuracy EUV metrology of PTB using synchrotron radiation," *Proceedings of SPIE*, vol. 4344, pp. 402–413, 2001.

[16] M. Krumrey and G. Ulm, *Nuclear Instruments & Methods in Physics Research, Section A: Accelerators, Spectrometers, Detectors, and Associated Equipment*, vol. 467-468, p. 1175, 2001.

[17] W. Görner, M. P. Hentschel, B. R. Müller, H. Riesemeier, M. Krumrey, G. Ulm, W. Diete, U. Klein, and R. Frahm, *Nuclear Instruments & Methods in Physics Research, Section A: Accelerators, Spectrometers, Detectors, and Associated Equipment*, vol. 467-468, p. 703, 2001.

[18] M. Gerlach, M. Krumrey, L. Cibik, P. Müller, H. Rabus, and G. Ulm, *Metrologia*, vol. 45, p. 577, 2008.

[19] J. Lubeck, B. Beckhoff, R. Fliegauf, I. Holfelder, P. Hönicke, M. Müller, B. Pollakowski, F. Reinhardt, and J. Weser, *Review of Scientific Instruments*, vol. 84, p. 045106, 2013.

[20] J. J. Rehr, S. I. Zabinsky, and R. C. Albers, "High-order multiple scattering calculations of x-ray-absorption fine structure," *Physical Review Letters*, vol. 69, p. 3397, 1992.

[21] L. Tröger, D. Arvanitis, K. Baberschke, H. Michaelis, U. Grimm, and E. Zschech, "Full correction of the self-absorption in soft-fluorescence extended x-ray-absorption fine structure," *Physical Review B*, vol. 46, no. 6, pp. 3283–3289, Août 1992.

[22] D. E. Cullen, J. H. Hubbell, and L. Kissel, "Epdl97: the Evaluated Photon Data Library, '97 Version"," *UCRL-50400*, vol. 6, no. 5, 1997, consultation date: 2015. [Online]. Available: http://www.llnl.gov/cullen1/document/epdl97/epdl97.pdf